

# iREVIEWS

STATE-OF-THE-ART REVIEW

## Advances in Parametric Mapping With CMR Imaging

Michael Salerno, MD, PhD,\*†‡ Christopher M. Kramer, MD\*†  
*Charlottesville, Virginia*

Cardiac magnetic resonance imaging (CMR) is well established and considered the gold standard for assessing myocardial volumes and function, and for quantifying myocardial fibrosis in both ischemic and nonischemic heart disease. Recent developments in CMR imaging techniques are enabling clinically-feasible rapid parametric mapping of myocardial perfusion and magnetic relaxation properties ( $T_1$ ,  $T_2$ , and  $T_2^*$  relaxation times) that are further expanding the range of unique tissue parameters that can be assessed using CMR. To generate a parametric map of perfusion or relaxation times, multiple images of the same region of the myocardium are acquired with different sensitivity to the parameter of interest, and the signal intensities of these images are fit to a model which describes the underlying physiology or relaxation parameters. The parametric map is an image of the fitted perfusion parameters or relaxation times. Parametric mapping requires acquisition of multiple images typically within a breath-hold and thus requires specialized rapid acquisition techniques. Quantitative perfusion imaging techniques can more accurately determine the extent of myocardial ischemia in coronary artery disease and provide the opportunity to evaluate microvascular disease with CMR.  $T_1$  mapping techniques performed both with and without contrast are enabling quantification of diffuse myocardial fibrosis and myocardial infiltration. Myocardial edema and inflammation can be evaluated using  $T_2$  mapping techniques.  $T_2^*$  mapping provides an assessment of myocardial iron-overload and myocardial hemorrhage. There is a growing body of evidence for the clinical utility of quantitative assessment of perfusion and relaxation times, although current techniques still have some important limitations. This article will review the current imaging technologies for parametric mapping, emerging applications, current limitations, and potential of CMR parametric mapping of the myocardium. The specific focus will be the assessment and quantification of myocardial perfusion and magnetic relaxation times. (*J Am Coll Cardiol Img* 2013;6:806–22)  
© 2013 by the American College of Cardiology Foundation

Cardiac magnetic resonance imaging (CMR) has emerged as a mature imaging modality and is considered the gold standard for quantification of myocardial mass, volumes, and function (1). Myocardial tagging and phase-contrast velocity imaging have been in use for over 20 years providing quantification of myocardial function and flow. While CMR has been used for tissue

From the \*Cardiovascular Division, Department of Medicine, University of Virginia Health System, Charlottesville, Virginia; †Department of Radiology and Medical Imaging, University of Virginia Health System, Charlottesville, Virginia; and the ‡Department of Biomedical Engineering, University of Virginia, Charlottesville, Virginia. Funding was received by grant NIH K23 HL112910-01. Dr. Salerno has received research support from Siemens. Dr. Kramer has received research equipment support from Siemens Healthcare and is a consultant for Synarc. Sherif Nageh, MD, served as the guest editor for this article.

characterization for many years, it is only with recent improvements in magnetic resonance imaging (MRI) scanner technology and parallel imaging reconstruction techniques that parametric mapping of perfusion or magnetic relaxation properties ( $T_1$ ,  $T_2$ , and  $T_2^*$ ) has become clinically feasible within a single breath-hold. To generate a parametric map of perfusion or relaxation times, multiple images of the same region of the myocardium are acquired with different sensitivity to the parameter of interest, and the signal intensities of these images are fit to a model that describes the underlying physiology or relaxation parameters. The parametric map is an image of the fitted perfusion parameters or relaxation times. Parametric mapping techniques are extending the range of unique tissue parameters that can be measured by CMR. Quantitative perfusion imaging techniques measure myocardial perfusion and perfusion reserve (MPR), demonstrating improved abilities to assess the extent of myocardial ischemia in multi-vessel disease (2). Pre- and post-contrast  $T_1$  mapping techniques can quantify diffuse myocardial fibrosis in hypertrophic and infiltrative cardiomyopathies (3-5).  $T_2$  mapping techniques are improving quantification of myocardial edema (6,7). Imaging of the  $T_2^*$  relaxation time, which is sensitive to magnetic field inhomogeneity, has become clinically useful in evaluation of myocardial iron overload and assessment of chelation therapy (8,9). This article will review the current imaging techniques, emerging applications, and the future potential and limitations of CMR for parametric mapping of the myocardium. It will specifically focus on assessment of myocardial perfusion, and magnetic relaxation times ( $T_1$ ,  $T_2$ , and  $T_2^*$ ).

### Quantification of Myocardial Perfusion

Most clinical perfusion imaging techniques only assess relative differences in myocardial perfusion. The single-photon emission computed tomography (SPECT) literature has established that measuring relative perfusion results in reduced sensitivity for the detection of left-main and 3-vessel coronary artery disease (CAD) as there may be no reference area with normal perfusion (10,11). Furthermore, there is growing interest in the ability to assess microvascular dysfunction in women and patients with diabetes or chest pain and nonobstructive CAD (12). Positron emission tomography (PET) is considered the current gold standard technique for quantitative perfusion imaging. Studies have shown that quantification of myocardial PET improves diagnostic

accuracy and provides a useful adjunct to assessment of regional perfusion abnormalities. Abnormal MPR by PET in the absence of obstructive CAD is associated with adverse cardiovascular outcomes (13). PET has a few disadvantages including high cost, limited ability to obtain tracers, poor spatial resolution, and exposure of patients to ionizing radiation (14). CMR has demonstrated potential for clinical quantitative perfusion imaging and would overcome some of the aforementioned limitations of PET for this application (15).

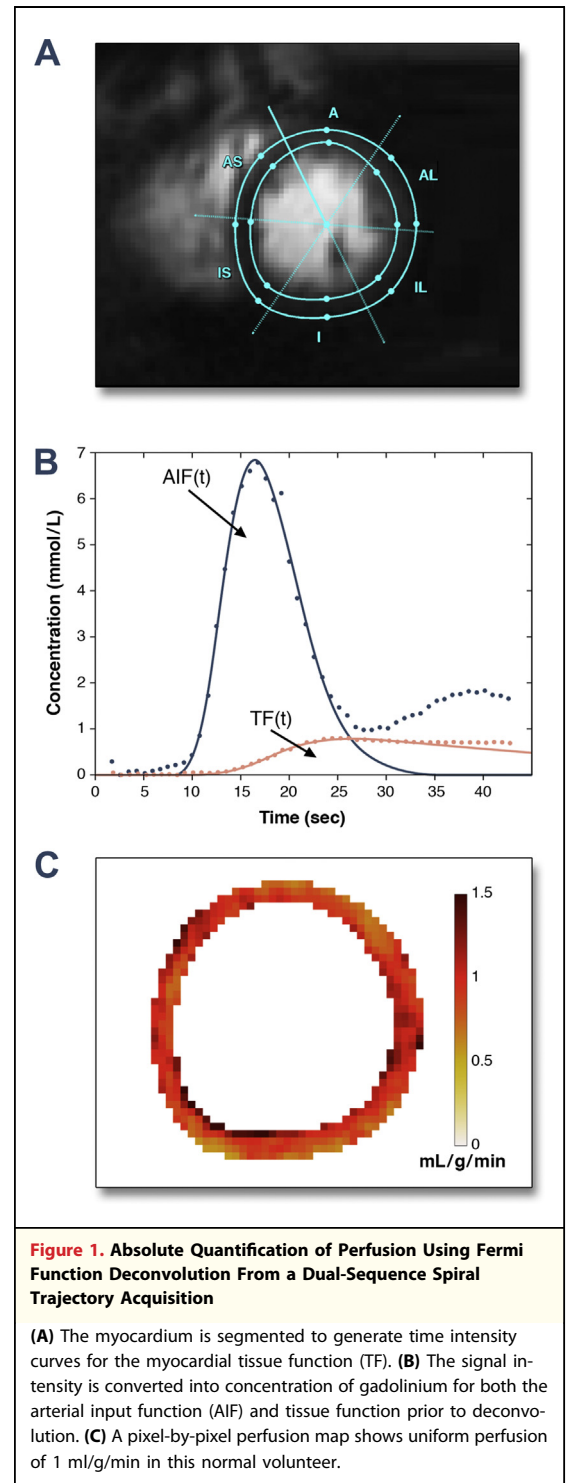
**CMR techniques for quantitative perfusion analysis.** In order to perform absolute quantification of myocardial blood flow, a quantifiable relationship must exist between the signal intensity changes in the image and underlying blood flow. First-pass myocardial perfusion techniques utilize gadolinium (Gd) chelates that shorten the  $T_1$  relaxation time of water (recovery of longitudinal magnetization) in proportion to the concentration of Gd using saturation-recovery (SR) pulse sequences to impart strong  $T_1$ -weighted (W) image contrast. In regions with normal blood flow there is an increased concentration of Gd resulting in a bright signal in the perfusion image, whereas in regions of reduced perfusion there are lower concentrations of gadolinium, resulting in a lower signal intensity. Typically 3 to 5 slice positions are imaged in a sequential fashion during each heartbeat over the 30 to 60 s of the first pass of the contrast agent. Multiple pulse sequences have been used for perfusion imaging and have their advantages and disadvantages (14). Parallel imaging with acceleration factors of 2 to 3 are routinely used (16) and multiple highly accelerated techniques have been evaluated in clinical studies (17). More recent techniques which exploit the spatial-temporal correlations in the series of first-pass perfusion imaging using techniques such as SENSitivity Encoding are enabling true 3-dimensional coverage of the ventricle with high spatial resolution (18). Compressed-sensing techniques, which rely on the compressibility of image data, or image sparsity, hold potential for even more acceleration of perfusion image acquisition (19). While any of these techniques can be used for quantification of myocardial perfusion, care must be taken to make sure that the techniques used do not disrupt the temporal evolution of the signal intensities.

### ABBREVIATIONS AND ACRONYMS

<b>AIF</b>	= arterial input function
<b>ASL</b>	= arterial spin labeling
<b>BOLD</b>	= blood oxygen dependent
<b>CAD</b>	= coronary artery disease
<b>CFR</b>	= coronary flow reserve
<b>CMR</b>	= cardiac magnetic resonance
<b>ECV</b>	= extracellular volume
<b>FFR</b>	= fractional flow reserve
<b>LGE</b>	= late gadolinium enhancement/enhanced
<b>MI</b>	= myocardial infarction
<b>MOLLI</b>	= Modified Look-Locker
<b>MPR</b>	= myocardial perfusion and perfusion reserve
<b>MRI</b>	= magnetic resonance imaging
<b>PET</b>	= positron emission tomography
<b>SNR</b>	= signal-to-noise ratio
<b>SR</b>	= saturation-recovery
<b>SSFP</b>	= steady-state free precession
<b>T<sub>2</sub>-Prep</b>	= T <sub>2</sub> magnetization-preparation
<b>TF</b>	= tissue function
<b>TSE</b>	= turbo spin echo
<b>Vd</b>	= volume of distribution

In order to quantify myocardial perfusion, 2 essential components must be measured accurately: 1) the AIF, which quantifies the concentration of Gd delivered from the left ventricle and aorta as a function of time; and 2) the tissue function (TF), which is related to the accumulation of contrast agent within the myocardium. Quantification of the arterial input function (AIF) requires special attention as the high concentration of Gd in the blood pool results in significant signal saturation resulting in improper determination of the AIF. This problem can be overcome using several different strategies. One approach is using a lower dose of contrast agent; however, this results in images with lower signal-to-noise ratio (SNR). Another is the “dual bolus” or “pre-bolus” technique where a low dose of Gd is used for quantification of the AIF and a second higher dose of contrast is used to determine the TF (20). This technique accurately quantifies both the AIF and TF, but it requires 2 boluses with different contrast concentrations, which may be impractical. A third approach involves utilization of a “dual sequence” approach, which uses a single high dose of contrast (21). A low resolution, low  $T_1$  sensitivity acquisition is performed in each heartbeat to quantify the AIF, while the standard pulse sequence is used to quantify the TF.

Once an accurate AIF and TF have been obtained, there are 2 main techniques to quantify perfusion, multicompartment kinetic modeling, and Fermi function deconvolution. With compartmental modeling, the forward flux of Gd from the blood to the myocardium ( $K_{trans}$ ) is taken to represent absolute myocardial blood flow (22). An important factor that is usually neglected is that the extraction of Gd, which is flow-dependent, is required to convert  $K_{trans}$  into a measurement of absolute perfusion. Also, the fact that Gd accumulates in the extravascular space is also not frequently accounted for by this analysis. With Fermi function deconvolution the central volume principle is used to describe the amount of Gd present within a region of myocardium (23). An empirical Fermi function is used for deconvolution and the initial amplitude of the Fermi function fit is proportional to myocardial perfusion. Figure 1 demonstrates the quantification of perfusion using Fermi function deconvolution of data acquired with a dual-bolus sequence. This technique is relatively robust to the effects of extracellular accumulation of the contrast agent at least during first pass of the contrast (24). Multiple other “model-independent techniques” have been used for deconvolution, and recently there have been studies comparing the relative merits of



the different techniques (25). Both of the techniques described previously have been shown to correlate with myocardial perfusion over a wide range of flow.

Arterial spin labeling (ASL) is an alternative technique for quantitative perfusion, which uses the water in blood as an endogenous contrast agent.

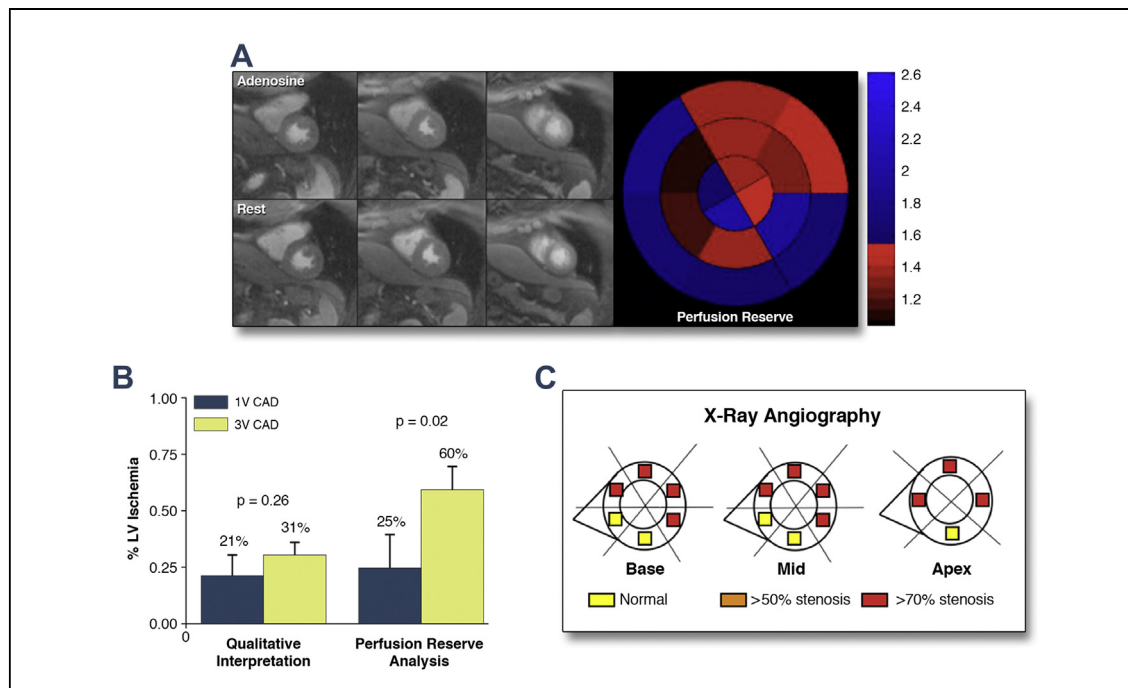


**Figure 2. Quantitative Perfusion May Be Useful in Determining Extent of Ischemia in Multivessel Disease**

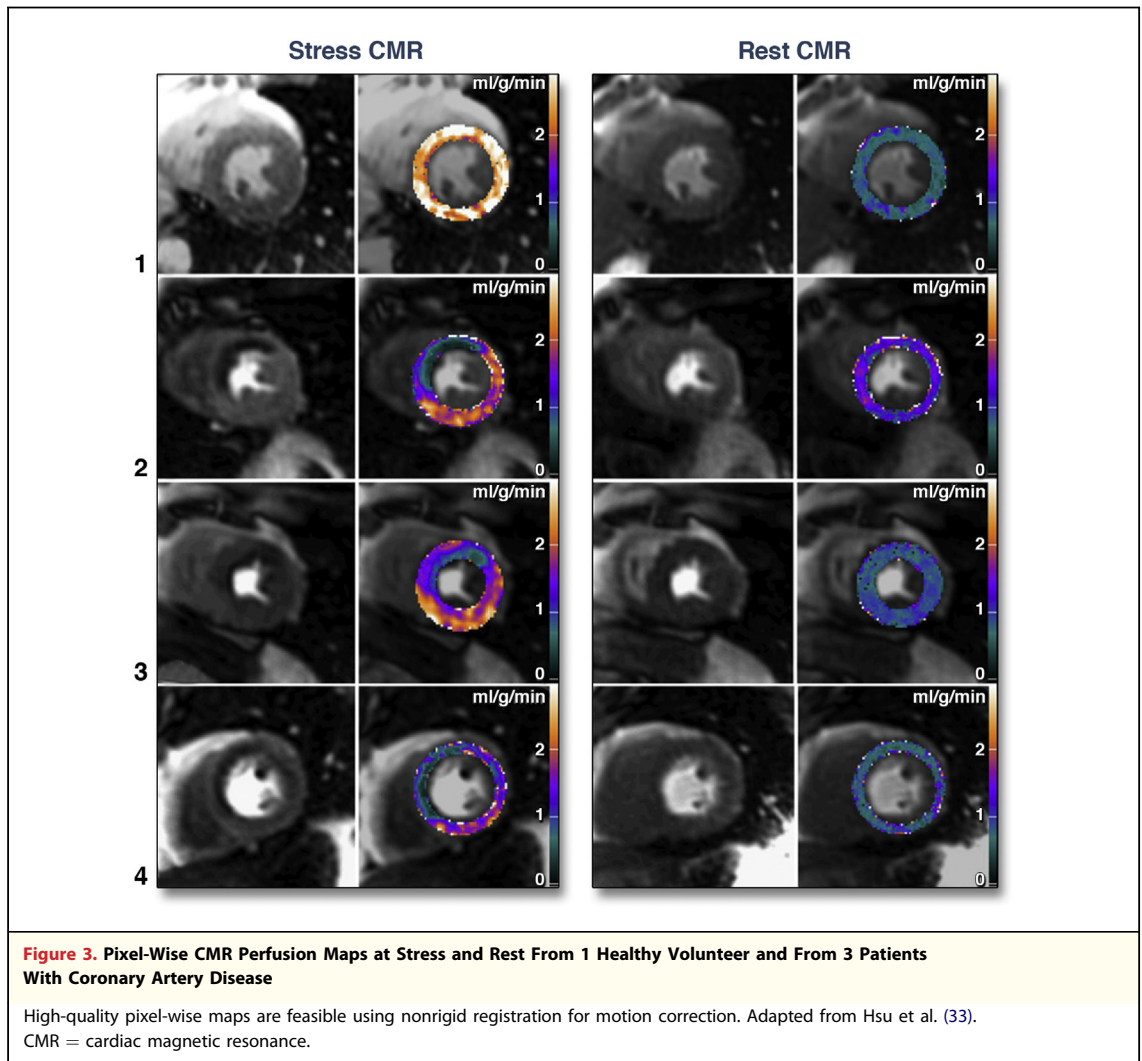
(A) Visual analysis of the stress images does not show a significant perfusion abnormality; however, quantification shows a region of reduced perfusion reserve corresponding to an abnormality found in the left anterior descending coronary artery at cardiac catheterization. (B) Although visual and quantitative analysis had similar diagnostic accuracy, quantitative analysis revealed a larger area of ischemia in 3-vessel disease as compared with single-vessel disease and may be important for quantifying the volume of ischemic myocardium. Adapted from Patel et al. (2). CAD = coronary artery disease.

The main limitation of ASL is poor SNR due to the small difference between the “labeled” and non-labeled acquisitions. This technique has been used to detect obstructive CAD; however, there are still some technical hurdles for the technique to have widespread clinical applicability (26). ASL may have utility in quantifying perfusion in more diffuse processes such as microvascular dysfunction, which may not require high spatial resolution.

**Clinical quantitative perfusion imaging.** Multiple studies have validated CMR perfusion imaging in experimental animal models with microspheres as the gold standard. CMR has also been validated in human subjects by direct comparison to PET and invasive measures of coronary flow reserve (CFR) and fractional flow reserve (FFR). A study of 19 healthy volunteers demonstrated strong correlation of both absolute perfusion ( $R = 0.86$ ) and MPR ( $R = 0.96$ ) between quantitative CMR using kinetic modeling and  $^{13}\text{N}$ -ammonia PET. However, there was an underestimate of peak perfusion by CMR as compared to PET (27).

Quantitative MPR was compared to CFR as assessed by coronary flow wire in a study of 20 patients with suspected CAD. This study demonstrated

a strong correlation between CMR and CFR ( $R = 0.86$ ) and a sensitivity of 88% and a specificity of 90% for predicting a  $\text{CFR} < 2$  (28). Quantitative CMR was also prospectively compared to FFR in 37 patients with suspected CAD who underwent FFR and coronary angiography (29). The study showed a reduced MPR of 1.54 for segments with  $\text{FFR} < 0.75$  and an MPR of 2.11 for segments with  $\text{FFR} > 0.75$ . A cutoff of 2.04 for MPR was highly sensitive (92.9%), but not specific (56.7%), for predicting an  $\text{FFR} < 0.75$ . Our group studied 41 subjects with known or suspected CAD using quantitative MPR by CMR as compared to x-ray angiography for detection of CAD and delineation of the extent of ischemic myocardium (Fig. 2) (2). While qualitative and quantitative analysis had similar diagnostic accuracy (83% vs. 80%) for detecting significant CAD, MPR detected a significantly higher burden of ischemia in 3-vessel disease as compared with single-vessel disease (60% vs. 25%,  $p = 0.02$ ). For visual analysis, there was no difference in the extent of detected ischemia between 3-vessel and single-vessel disease (31% vs. 21%,  $p = 0.26$ ). A recent study has directly compared the performance of quantitative CMR at 1.5- and 3-T field strengths to detect an



FFR  $< 0.8$  in 34 patients with known or suspected CAD. This study demonstrated a higher receiver-operating characteristic area under the curve (0.963 vs. 0.645,  $p < 0.001$ ), sensitivity (90.5% vs. 61.9%), and specificity (100% vs. 76.9%) at 3-T versus 1.5-T (30).

**Current limitations and future potential.** Several factors have hampered the widespread clinical application of quantitative perfusion CMR. One is the limited spatial coverage (typically 3 to 4 slices) as compared with PET. However, new imaging pulse sequences using spatiotemporal parallel techniques have demonstrated the potential for rapid high resolution and 3-dimensional coverage of the myocardium (18). Furthermore, spiral or radial techniques hold promise for further acceleration of image acquisition (31,32). Increased field strength from 1.5- to 3-T may also improve SNR and diagnostic performance. The lack of robust automated tools for

image registration and quantification has limited the applicability of quantitative analysis to research settings. However, nonrigid registration techniques have recently been applied to perform point-by-point quantification (Fig. 3) (33). The final barrier is to demonstrate that perfusion quantification has additional benefit over visual analysis or semi-quantitative techniques. One of the justifications for absolute quantification has been improved detection of 3-vessel disease; however, the improved spatial resolution of CMR may provide sufficient gradient of perfusion to enable adequate visual analysis. Multiple studies have demonstrated a high diagnostic accuracy of CMR stress imaging without the complex data analysis required for quantification, and the incremental benefit of absolute quantification still needs to be established in larger clinical studies (34).

**Quantification of myocardial  $T_2^*$  relaxation times.** Quantification of  $T_2^*$  relaxation times is arguably the

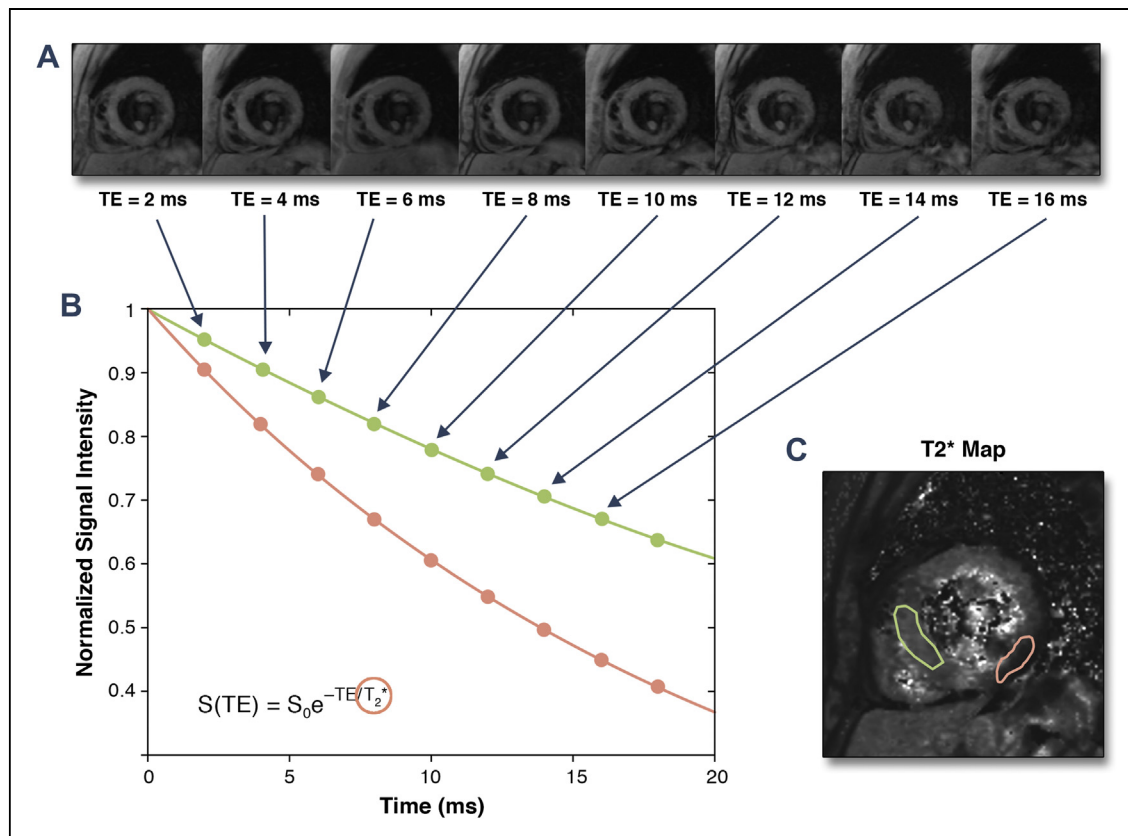


**Figure 4. Calculation of T<sub>2</sub>\* Maps in a Normal Subject**

(A) A set of gradient echo images acquired with different echo times (TE) from 2 to 18 ms are acquired. As the TE is increased the signal intensity decreases due to static field inhomogeneities resulting in T<sub>2</sub>\* decay. (B) The data from each pixel are fit to a T<sub>2</sub>\* decay curve. Pixels with longer T<sub>2</sub>\* decay more slowly (pink curve) as compared to regions with shorter T<sub>2</sub>\* (green curve). (C) The T<sub>2</sub>\* map shows a region of reduced T<sub>2</sub>\* in the inferolateral wall, which is caused by a susceptibility artifact and can be seen even in normal subjects.

most clinically established quantitative CMR tissue characterization technique as it has revolutionized the detection and monitoring of iron-overload cardiomyopathy. T<sub>2</sub>\* is the transverse relaxation time in the presence of static magnetic field inhomogeneities. T<sub>2</sub>\* mapping techniques enable detection of spatially varying differences in T<sub>2</sub>\* relaxation times and can be used to detect the presence of hemorrhage in acute myocardial infarction (MI). T<sub>2</sub>\* mapping techniques also can detect changes in myocardial oxygenation based on the blood oxygen dependent (BOLD) effect, which results from the difference in magnetic state between oxyhemoglobin (diamagnetic) and deoxyhemoglobin (paramagnetic) as deoxyhemoglobin reduces the T<sub>2</sub>\* of blood.

**CMR techniques for quantifying myocardial T<sub>2</sub>\*.** To create a myocardial T<sub>2</sub>\* map, multiple images with different sensitivities to T<sub>2</sub>\* must be acquired. This is typically achieved by collecting gradient echo images with different echo times yielding images with signal intensities which follow a T<sub>2</sub>\* relaxation curve.

The most commonly used pulse sequence for data acquisition are a multiecho segmented gradient echo technique which typically collects data at 8 different echo times ranging from 2 to 20 ms (Fig. 4) (35). Image data are acquired directly after the R-wave, which further reduces artifacts from blood flow and myocardial motion. T<sub>2</sub>\* measurements have primarily been measured in the intraventricular septum as this area is typically free from magnetic susceptibility artifacts which corrupt the long echo time images, particularly in the lateral wall.

**Clinical application of T<sub>2</sub>\* mapping techniques.** The T<sub>2</sub>\* relaxation time is shortened by magnetic field inhomogeneities induced by myocardial iron deposition. A reduction of T<sub>2</sub>\* to <20 ms is consistent with the diagnosis of iron overload cardiomyopathy (8). The presence of abnormal T<sub>2</sub>\* is the most important predictor of future requirement for chelation therapy. Changes in the myocardial T<sub>2</sub>\* have been used as a surrogate endpoint of several clinical trials of chelation therapy in transfusion dependent

thalassaemia major patients (9). Quantitative  $T_2^*$  mapping has been applied to the detection of myocardial hemorrhage in acute MI. In a study of 62 patients with acute reperfused MI, 62% of subjects had evidence of microvascular obstruction seen on late gadolinium enhanced (LGE) imaging, however only 20% of patient had hemorrhage as indicated by  $T_2^* < 30$  ms (36).  $T_2^*$  mapping has been used to probe the BOLD effect in ischemic heart disease. An early study of  $T_2^*$  mapping in 16 healthy volunteers and 16 patients with known single-vessel CAD demonstrated that volunteers had a  $T_2^*$  of 35 ms at rest, which increased to 40 ms with dipyridamole infusion due to the reduction in deoxygenated hemoglobin during hyperemia. In subjects with single-vessel CAD, there were regional reductions in  $T_2^*$  at rest in the regions supplied by stenotic arteries, and these differences increased significantly during dipyridamole (37). In another study, 46 patients with known or suspected CAD underwent BOLD  $T_2^*$  mapping at rest and during adenosine stress at 3-T. BOLD CMR at rest demonstrated significantly lower  $T_2^*$  values for ischemic segments ( $26.7 \pm 11.6$

ms) as compared with normal ( $31.9 \pm 11.9$  ms) segments. A stress  $T_2^* < 33.8$  had 78% sensitivity and 68% specificity on a per patient basis to detect significant CAD (38).

**Potential clinical pitfalls and solutions.** Care must be taken when interpreting regional differences in  $T_2^*$  from maps as the  $T_2^*$  can be abnormally short in certain regions of the heart even in normal subjects due to macroscopic magnetic field inhomogeneity. This is particularly problematic in the inferolateral wall. For assessment of iron overload, which diffusely affects the myocardium, measurement of the  $T_2^*$  time in the intraventricular septum is preferred.

### Quantification of Myocardial $T_2$ Relaxation Times

It has been long recognized that  $T_2$  relaxation times are sensitive to myocardial edema and are known to be elevated in acute MI (39), myocarditis (40), sarcoidosis (41), and in cardiac allograft rejection (42).  $T_2$  is the relaxation time for transverse magnetization and is prolonged in regions of edema or inflammation. The current standard  $T_2$ -weighted

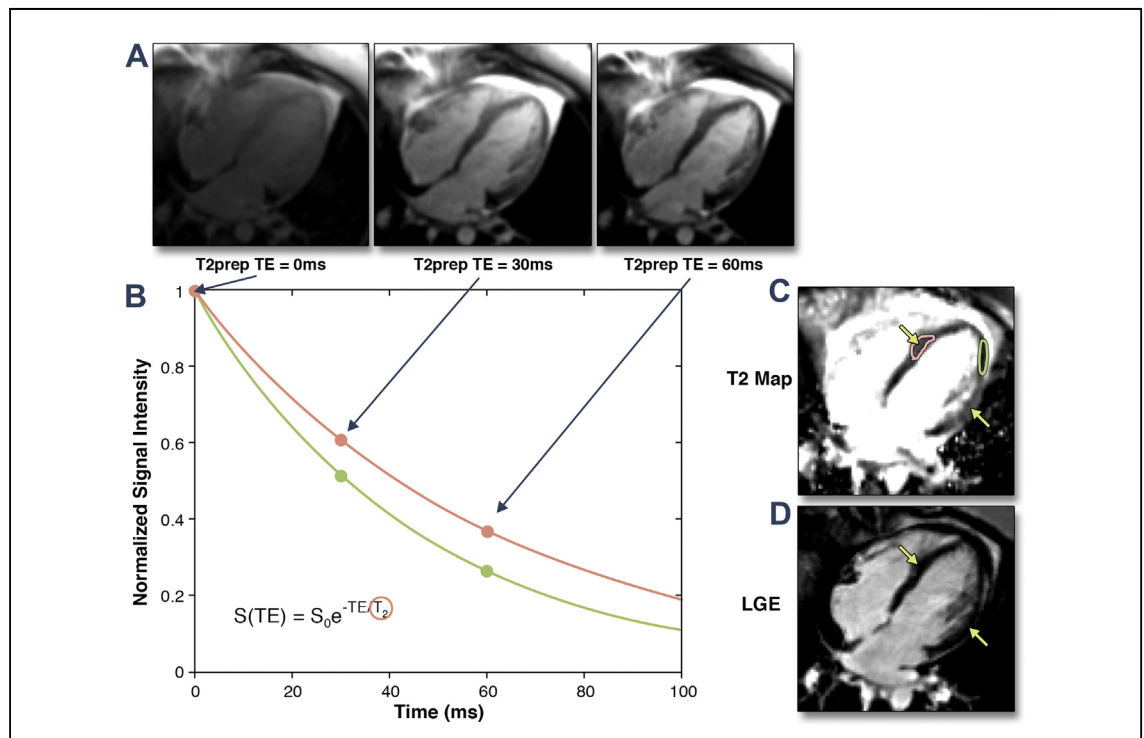


**Figure 5. Calculation of  $T_2$  Maps Using a  $T_2$ -Prep Pulse Sequence in a Patient With Atypical Takotsubo Cardiomyopathy**

(A) Multiple images with  $T_2$  magnetization-preparation ( $T_2$ -Prep) with different echo times (TE) are acquired. As the TE is increased for this spin echo-based preparation, the myocardial signal intensity decreases due to  $T_2$  decay. (B) The data from each pixel are fit to a  $T_2$  decay curve. Pixels with longer  $T_2$  (pink curve) decay more slowly than regions with shorter  $T_2$  (green curve). (C) The  $T_2$  map shows a region of edema (yellow arrows and pink region of interest) in this patient. (D) The absence of late gadolinium enhancement (LGE) confirms the diagnosis of atypical Takotsubo cardiomyopathy.

dark-blood turbo spin echo sequences (TSE) have significant limitations, particularly for semi-quantitative evaluation. Factors such as incomplete blood suppression with dark-blood techniques, regional variations in signal intensity from coil inhomogeneities, and signal loss from myocardial contraction and relaxation during acquisition are significant challenges for this technique in clinical practice. In addition, as  $T_2$ -weighted images are inherently nonquantitative, semiquantitative techniques have relied on defining abnormal  $T_2$  by a number of standard deviations of signal intensity over that of remote myocardium, which can be problematic when there is no remote “normal” reference region. In the last few years, techniques capable of rapid measurement of the myocardial  $T_2$  relaxation time have emerged and may have important advantages over the prior semiquantitative techniques.

**CMR techniques for quantifying  $T_2$  relaxation times.** In order to quantify myocardial  $T_2$  relaxation times, multiple images with different sensitivities to  $T_2$  need to be acquired. This is typically achieved by collecting spin-echo images with different echo times yielding images with signal intensities that follow a  $T_2$  decay curve (Fig. 5). For cardiac  $T_2$  mapping applications 2 different types of sequences have been employed: 1) dark-blood TSE-based pulse sequences; and 2) bright-blood  $T_2$  magnetization-preparation ( $T_2$ -Prep)-based pulse

sequences. Both free-breathing navigator-gated acquisition and breath-hold strategies have been utilized.

TSE-based  $T_2$ -mapping techniques collect images at multiple echo times providing multiple points along the  $T_2$  relaxation curve for data fitting. TSE pulse sequences are sensitive to ghosting artifacts due to blood flow and dark-blood preparation must be utilized with these strategies. Furthermore, these sequences have some inherent sensitivity to motion, which needs to be accounted for to accurately quantify  $T_2$ . The effects of coil inhomogeneity are eliminated during the  $T_2$  fitting procedure. The  $T_2$ -prep pulse sequence consists of a spin-echo-like preparation module to impart the  $T_2$ -weighted contrast and a readout scheme to rapidly collect the image data (43). Typically a rapid steady-state free precession (SSFP) readout is used, which is less sensitive to some of the artifacts, which limit TSE-based techniques. By acquiring multiple images, each with a different  $T_2$ -Prep duration, a  $T_2$  map can be determined (Fig. 5) (44,45). These techniques demonstrate an approximately 10% overestimate of  $T_2$  relative to reference techniques, likely due to the SSFP readout, which induces mixed  $T_1$  and  $T_2$  contrast (44).

**Clinical application of  $T_2$  mapping techniques.**  $T_2$  mapping techniques have demonstrated utility for evaluation of a variety of cardiac pathologies. The edematous territory measured by  $T_2$ -weighted

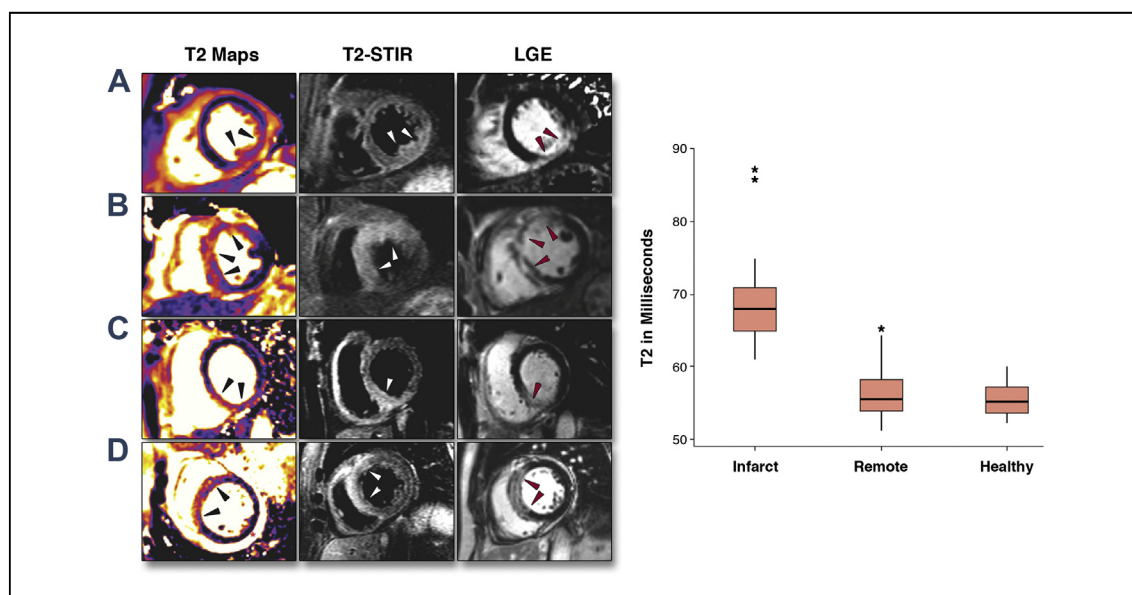
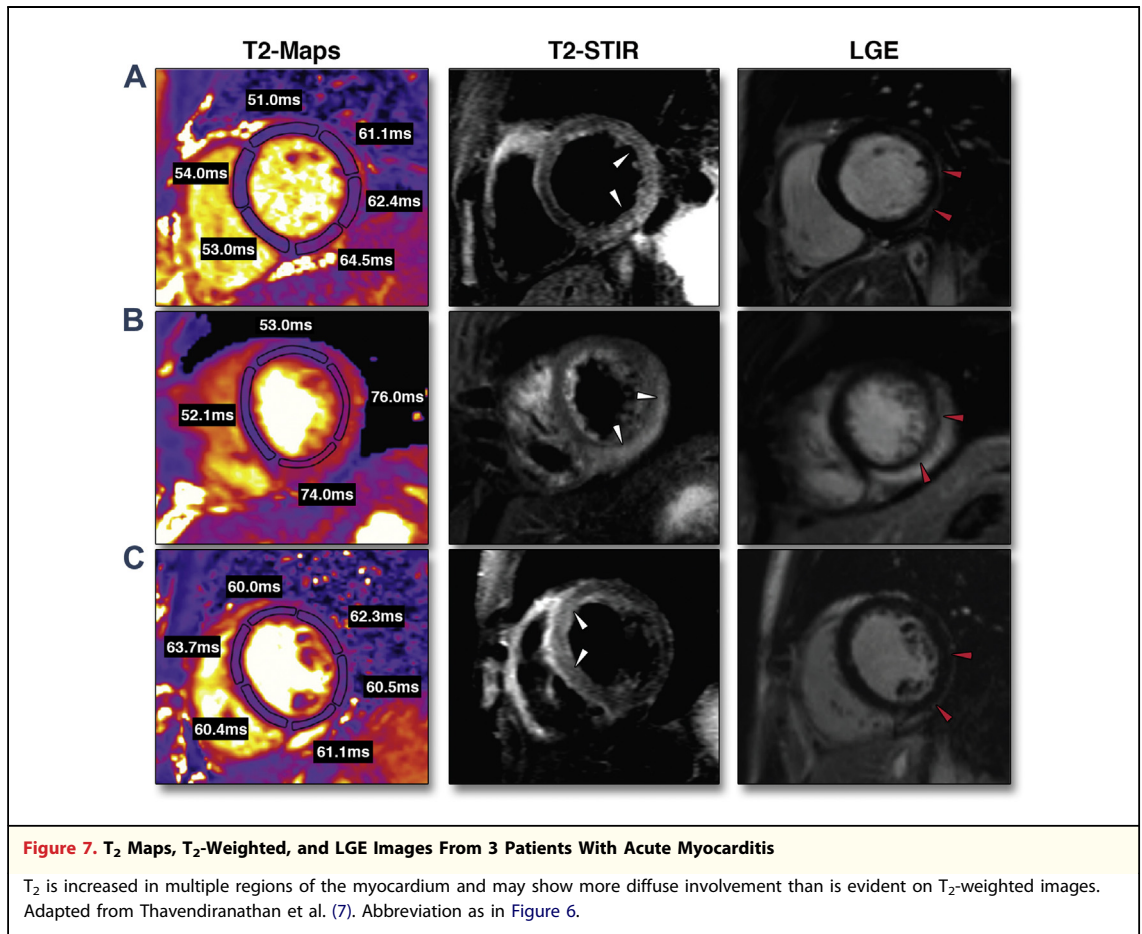


**Figure 6.  $T_2$  Mapping of Edema in Acute Myocardial Infarction**

(A)  $T_2$  maps,  $T_2$ -weighted, and late gadolinium enhanced (LGE) images from patients with acute myocardial infarction. (B) The  $T_2$  relaxation time was significantly increased in the region of the infarct as compared to remote and healthy myocardium. Adapted from Verhaert et al. (6).



imaging and T<sub>2</sub> mapping has been shown to correlate with the region of ischemic injury in a canine model of MI (46,47). This has stimulated considerable clinical interest in using T<sub>2</sub>-weighted imaging to assess myocardial salvage (48). A T<sub>2</sub>-Prep SSFP-based mapping technique was used to evaluate 27 patients with acute MI and 21 normal volunteers, demonstrating that the average T<sub>2</sub> in edematous myocardium was 69 ms compared with 56 ms in remote (Fig. 6) and 55 ms in normal volunteers (6). Importantly, edema was detected in 26 of 27 patients with T<sub>2</sub> mapping, whereas conventional short tau inversion recovery images were negative in 7 patients and uninterpretable in 2 cases.

In a study of 30 patients, T<sub>2</sub> mapping techniques have also demonstrated increased T<sub>2</sub> in the involved segments of myocardium in patients with acute inflammatory diseases including myocarditis and Takotsubo cardiomyopathy (Fig. 7) (7). In both pathologies there was no difference in the T<sub>2</sub> of the remote myocardium as compared with

controls. A T<sub>2</sub> cutoff of 59 ms had a sensitivity of 94% and specificity of 97% for identifying affected myocardium. Conventional T<sub>2</sub>-weighted images were uninterpretable in 7 subjects because of artifacts and did not demonstrate abnormalities in 2 subjects with abnormal T<sub>2</sub> values by T<sub>2</sub> mapping. Bright blood T<sub>2</sub>-Prep SSFP images did not show a clear region of increased signal intensity in 13 of 30 subjects. This study demonstrates that T<sub>2</sub> mapping may improve the ability to differentiate edematous myocardium over T<sub>2</sub>-weighted techniques.

T<sub>2</sub> mapping has also been used for the assessment of iron-overload cardiomyopathy (49). The superparamagnetic properties of iron result in a shortening of both T<sub>2</sub> and T<sub>2</sub><sup>\*</sup> relaxation times resulting in more rapidly decaying transverse magnetization which can be detected by CMR. T<sub>2</sub> mapping has 2 potential advantages over T<sub>2</sub><sup>\*</sup> mapping in that pulse sequences for determination of T<sub>2</sub> are less sensitive to static magnetic field inhomogeneities and typically produce images of higher SNR. In a

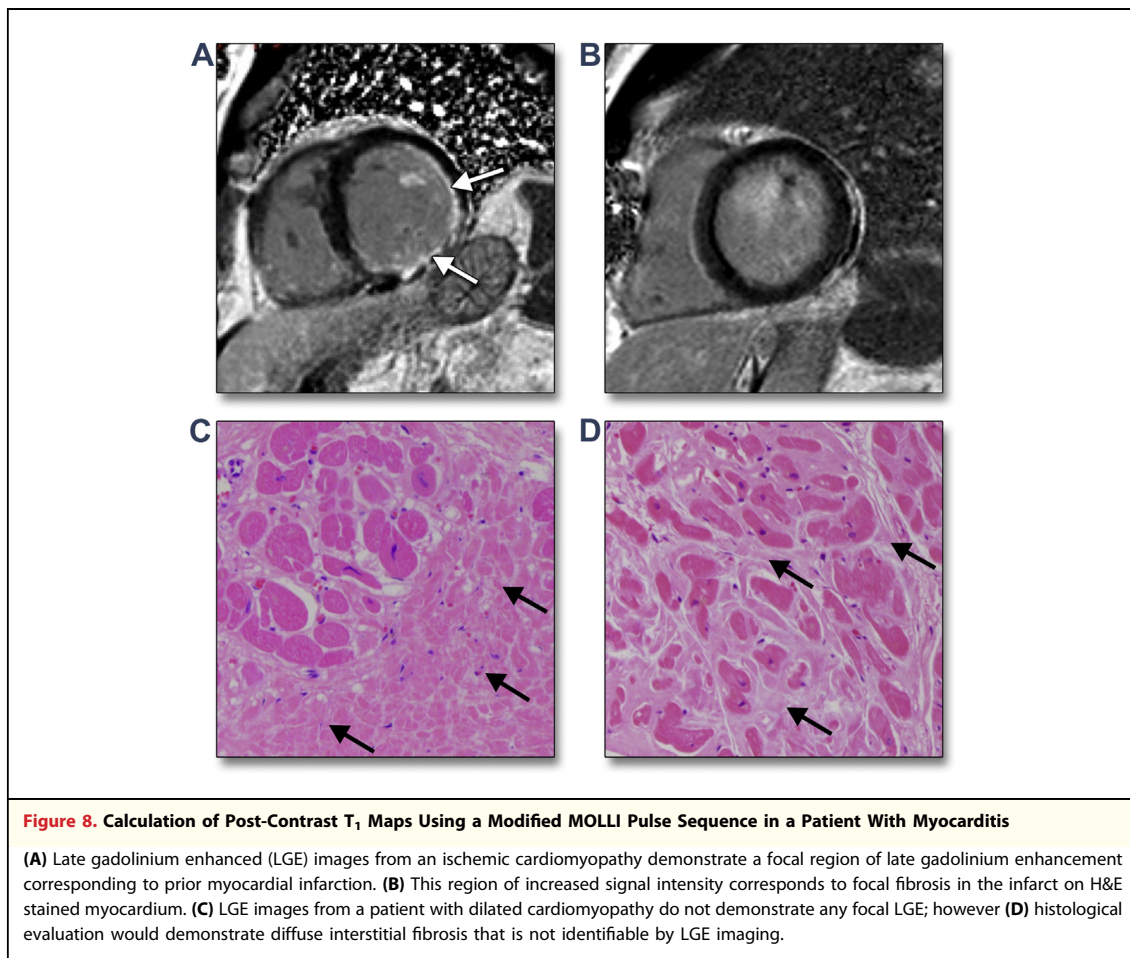


**Figure 8. Calculation of Post-Contrast  $T_1$  Maps Using a Modified MOLLI Pulse Sequence in a Patient With Myocarditis**

(A) Late gadolinium enhanced (LGE) images from an ischemic cardiomyopathy demonstrate a focal region of late gadolinium enhancement corresponding to prior myocardial infarction. (B) This region of increased signal intensity corresponds to focal fibrosis in the infarct on H&E stained myocardium. (C) LGE images from a patient with dilated cardiomyopathy do not demonstrate any focal LGE; however (D) histological evaluation would demonstrate diffuse interstitial fibrosis that is not identifiable by LGE imaging.

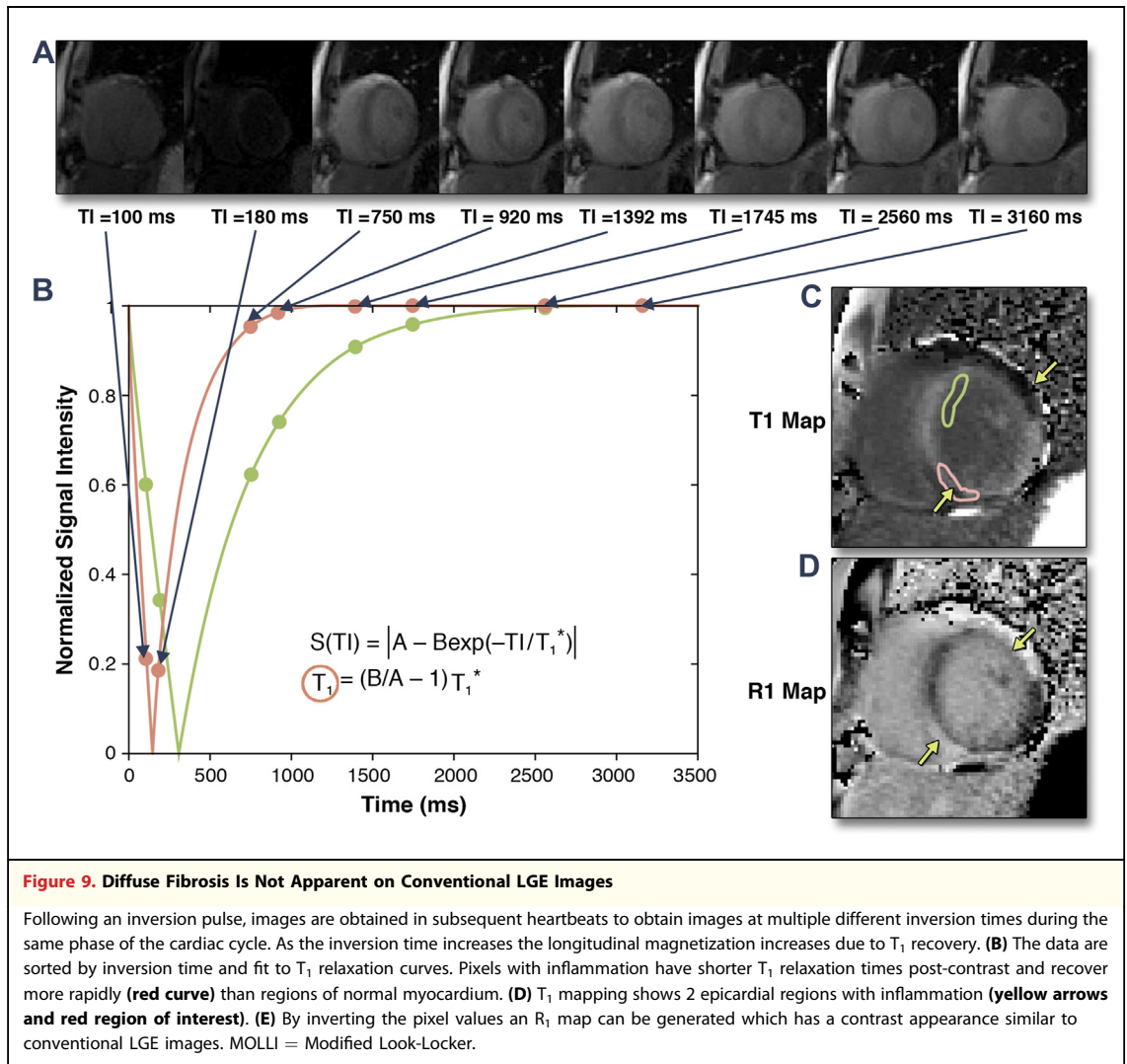
study of 136 patients with thalassaemia, a linear relationship has been demonstrated between  $T_2$  and  $T_2^*$  ( $R = 0.89$ ) in subjects with iron overload with similar diagnostic utility for detecting iron overload (49).

**Potential clinical pitfalls and solutions.** Care must be taken when comparing absolute  $T_2$  relaxation times between data acquired with different techniques as biases in the absolute numbers may occur between different sequences or patient-related factors. For the  $T_2$ -Prep mapping sequence, in a tachycardiac patient, incomplete  $T_1$  relaxation between each image acquisition may introduce some bias to the measured  $T_2$ -weighted images. This effect can be minimized by increasing the number of heartbeats between images (i.e., from 3 to 4 relaxation beats) to enable more time for  $T_1$  relaxation. TSE-based pulse sequences can also have some errors in accurate  $T_2$  determination by introducing some  $T_1$  dependence to the values. An additional problem is that current mapping sequences have limited spatial resolution as compared

to  $T_2$ -weighted images; however, this problem is likely to be overcome by improved pulse sequences and reconstruction techniques.

#### Quantification of $T_1$ Relaxation Times and Volume of Distribution of Gadolinium

LGE imaging has become the gold standard technique for imaging focal myocardial fibrosis in CAD and nonischemic cardiomyopathies (50,51). However, cardiac pathologies characterized by diffuse myocardial fibrosis cannot be evaluated adequately by LGE, as there are no reference regions of normal myocardium. Figure 8 shows LGE images and histology from MI and dilated cardiomyopathy. In MI, LGE images show focal enhancement corresponding to the dense focal fibrosis in the infarct, whereas in dilated cardiomyopathy LGE images may not show any enhancement despite the presence of significant interstitial fibrosis.  $T_1$  mapping techniques following Gd injection have demonstrated potential for evaluation of diffuse myocardial fibrosis and myocardial



infiltration. However, the  $T_1$  of the myocardium is a function not only of the amount of fibrosis, but also of Gd dose, clearance rate, and time after injection. There has been growing interest in assessing the volume of distribution of Gd, or extracellular volume (ECV), as a noninvasive marker of fibrosis by performing  $T_1$  mapping before and after either a continuous infusion or bolus injection of Gd. The Vd of Gd has also been used as a noninvasive marker of cardiac amyloidosis (52). Noncontrast  $T_1$  mapping, also referred to as native- $T_1$  mapping, has demonstrated potential for assessing myocardial edema in MI similar to work that has been done with  $T_2$ -weighted techniques (47). Noncontrast  $T_1$  values are increased in hypertrophic and dilated cardiomyopathy reflecting fibrosis (53), and in cardiac amyloidosis reflecting the presence of infiltration by amyloid protein (52,54,55).  $T_1$  mapping and Vd

measurements may also have potential for better delineation of peri-infarct zones and for providing a more quantitative assessment of myocardial scarring.

#### CMR Techniques for Quantifying $T_1$ Relaxation Times

There have been a variety of techniques that have been used to quantify myocardial  $T_1$  values (3–5, 56–58). The simplest but least efficient method is to collect a single image with a given sensitivity to  $T_1$  on each of multiple separate breath-holds and fit the signal intensities to the  $T_1$  recovery curve as shown schematically in Figure 9. This allows a  $T_1$  map to be determined during a specific phase of the cardiac cycle but is time consuming because it requires multiple breath-holds and may be subject to image misregistration between breath-holds. Two

techniques are available which acquire all of the data for a  $T_1$  map in a single breath-hold. The traditional Look-Locker technique collects image data continuously to create images at different time points following a  $T_1$ -weighted inversion preparation. A limitation of the traditional Look-Locker techniques is that the heart is in a different phase of the cardiac cycle on each image, precluding mapping of a specific slice as there may be significant through plane motion (59). The Modified Look-Locker (MOLLI) pulse sequence is a modification to the Look-Locker sequence in which single-shot images are obtained in diastole with 11 different  $T_1$  sensitivities over 17 heartbeats. The data from these diastolic source images are fit to the  $T_1$  recovery function to create a  $T_1$  map (Fig. 9). The MOLLI technique is reproducible, and produces source images with high SNR (60,61). A limitation of the standard MOLLI pulse sequence is the requirement of 17 heartbeats for data acquisition, which may result in a breath-hold that is too long for some patients. Several modifications have been proposed to reduce the breath-hold duration needed to collect the data and to reduce the heart-rate dependence (62,63). Furthermore, robust nonrigid registration has been introduced, which minimizes the effect of motion between the images collected on different heartbeats (64). The majority of recently published  $T_1$  mapping research has utilized 1 of the 3 techniques, or some variation thereof.

**CMR protocols for determining the volume of distribution of Gd.** By measuring  $T_1$  before and after either a bolus injection or equilibrium infusion of Gd, the apparent ECV can be determined by calculating the Vd of Gd (3,5,58,65). For the continuous infusion method, Gd is given as a continuous low dose infusion until the  $T_1$  in the myocardium and blood pool are constant. The Vd can then be directly determined from the  $T_1$  values obtained pre-contrast and at equilibrium according to the following equation (5,65).

$$ECV = (1 - Hct)\lambda = (1 - Hct) \frac{T_{1post\_myo} - T_{1pre\_myo}}{T_{1post\_blood} - T_{1pre\_blood}}$$

The bolus injection method relies on the assumption that the exchange between the blood pool and myocardium is fast with respect to Gd clearance from the blood such that there is equilibrium between the concentration of Gd in the blood pool and myocardium at each time point following Gd administration (3,58). The equivalence of these 2 approaches has been demonstrated (62,66).

**Clinical application of  $T_1$  mapping techniques.** The reported normal  $T_1$  relaxation times for the myocardium at 1.5-T range between 900 and 1,100 ms with some variation based on technique (59-61,63,66,67). Pre-contrast measurement of  $T_1$  should be increased in myocardial edema similar to  $T_2$  due to the increase in free water content of the tissue. A study of 8 patients who underwent pre-contrast  $T_1$  mapping demonstrated an 18% increase in  $T_1$  in infarcted regions (68). The area of increased  $T_1$  pre-contrast had a larger spatial extent as compared to the region of LGE (68). Pre-contrast  $T_1$  measurements have been compared to  $T_2$  measurements as an alternative for assessing the "area at risk" following acute ischemic injury and produce results similar to microsphere measurements (47). Pre-contrast  $T_1$  times are prolonged in both the myocardium and blood pool of subjects with amyloidosis as compared to normal volunteers (52,55). A recent study of 53 patients with AL amyloidosis demonstrated a significant prolongation of non-contrast  $T_1$  time in cardiac light-chain amyloidosis patients ( $1,140 \pm 61$  ms) as compared to 36 normal subjects ( $958 \pm 20$  ms). A  $T_1$  cutoff of 1,020 yielded 92% accuracy for identifying patients with possible or definite cardiac involvement (54). There was no significant difference in non-contrast  $T_1$  values between the controls and 17 subjects with aortic stenosis ( $979 \pm 51$  ms). Native  $T_1$  was also shown to be prolonged in cardiomyopathy in a study of 25 patients with known hypertrophic cardiomyopathy and 27 subjects with non-ischemic dilated cardiomyopathy as compared to 30 control subjects (53).

$T_1$  mapping post-contrast has demonstrated potential for evaluation of MI. In the same aforementioned study of 8 subjects with MI who underwent  $T_1$  mapping pre-contrast, there was a 27% reduction in post Gd contrast  $T_1$ , with a spatial extent which correlated well with LGE, demonstrating that  $T_1$  mapping could be an alternative for quantifying MI (68). An image of  $R_1$ , which is defined as  $1/T_1$ , will have an appearance similar to conventional LGE images where regions of fibrosis or infiltration are bright (Figs. 9C and 9D).

$T_1$  mapping has demonstrated the potential for assessing diffuse fibrosis and infiltration. In a study of 25 patients with heart failure, the  $T_1$  times in the myocardium after Gd contrast were reduced compared to 20 normal controls, and the post-contrast  $T_1$  times were correlated with the histological severity of fibrosis in 9 subjects who underwent myocardial biopsy (4). This study demonstrated that post-contrast  $T_1$  mapping could potentially be used

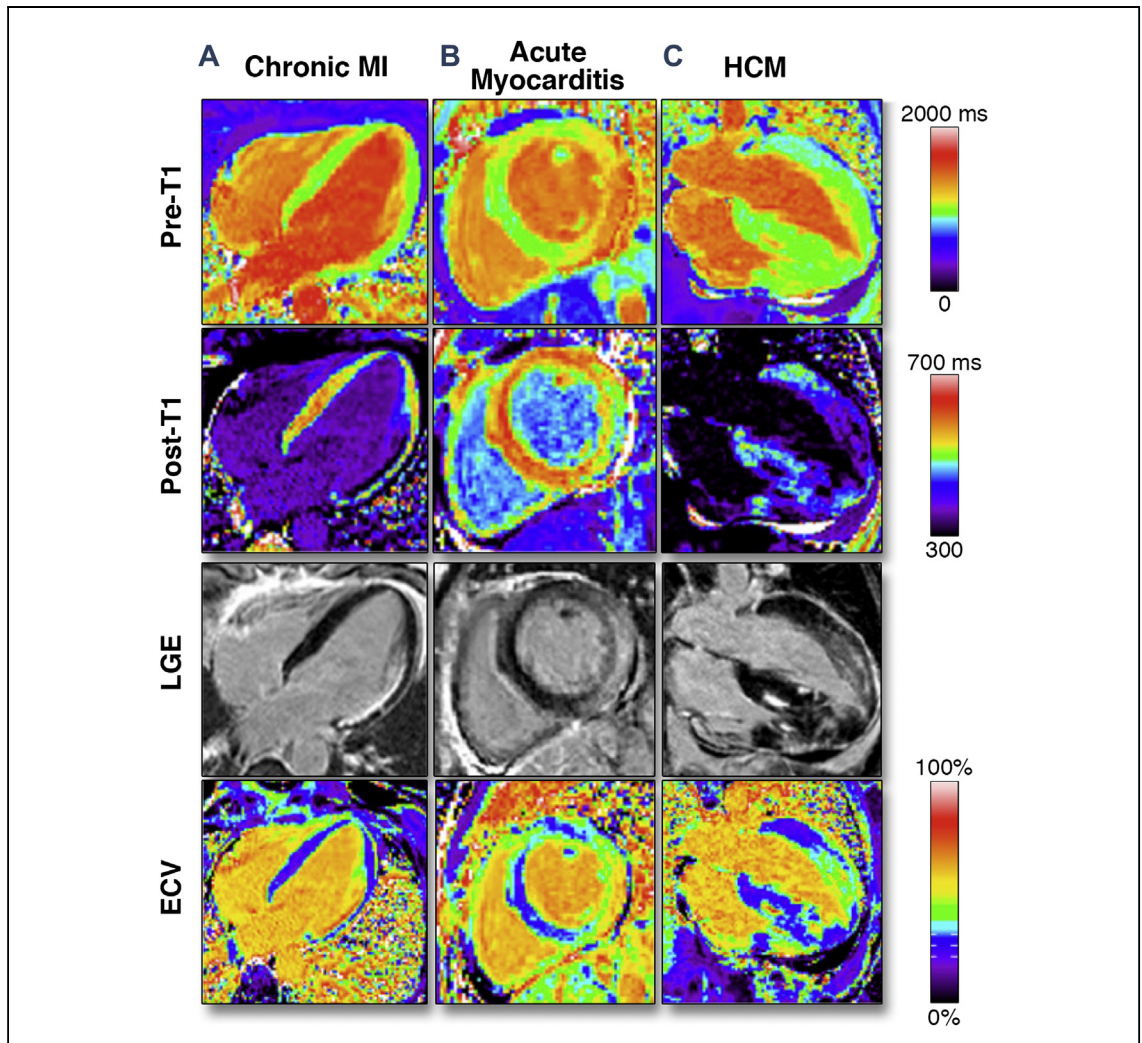


**Figure 10. Mapping of Myocardial Extracellular Volume**

Examples illustrating excellent agreement between late gadolinium enhancement (LGE) and extracellular volume (ECV) in cases of focal abnormalities in myocardial ECV. Pre-contrast  $T_1$ -maps (**top row**), post-contrast  $T_1$  maps (**second row**), late gadolinium enhancement (**third row**), and ECV maps (**bottom row**) for patients with (A) chronic myocardial infarction (MI), (B) acute myocarditis, and (C) hypertrophic cardiomyopathy (HCM). Adapted from Kellman et al. (71).

to evaluate diffuse fibrosis in cardiomyopathy. A study of 54 heart failure patients undergoing endomyocardial biopsy demonstrated a reduction in the 10-min post-contrast  $T_1$  time in the heart failure subjects as compared with 13 controls. In heart failure, the post-contrast  $T_1$  time was inversely correlated with the histological severity of fibrosis (69).  $T_1$  mapping post-contrast has also shown potential for the evaluation of cardiac amyloidosis (70). In 29 patients with proven cardiac amyloidosis a  $T_1$  difference of 23 ms between the subepicardium and subendocardium at 2 min after Gd administration predicted mortality in amyloidosis with 85% accuracy (70). In a study of 5 patients with amyloidosis, there

was also a smaller difference in  $T_1$  relaxation times between the blood pool and myocardium  $17.1 \pm 54.3$  ms versus  $136.1 \pm 18.4$  ms at 20 min after contrast administration as compared with 8 controls (52).

By measuring  $T_1$  before and after either a bolus or equilibrium infusion of Gd, the partition coefficient and volume of distribution of Gd can be assessed, and they are proportional to the ECV (Fig. 10). The ECV of normal myocardium has been reported to be in the range of 24% to 28% (56,62,66,71). Assessment of Vd or the partition coefficient lambda has been used to assess diffuse fibrosis in different cardiac pathologies. In 9 patients with dilated cardiomyopathy, the Vd of Gd was found to be significantly increased in

patients with both familial and dilated cardiomyopathy (3). Similar findings were demonstrated in congenital heart disease with myocardial dysfunction (56). Validation of the correlation between the Vd and histological evidence of myocardial fibrosis has been performed in 18 subjects with aortic stenosis undergoing aortic valve replacement and in 18 patients with HCM undergoing surgical myectomy using a multi-breath-hold equilibrium infusion  $T_1$  technique (5). Given the prognostic data available in HCM for the evaluation of focal fibrosis with LGE, it is likely that  $T_1$  mapping may provide additional disease in this disease as it reflects both focal and diffuse fibrosis (72).

The Vd and the partition coefficient of Gd are markedly increased in amyloid cardiomyopathy with expansion of the extracellular space due to amyloid protein deposition (55,73). The degree of change in Vd is much larger than the changes in the individual  $T_1$  measurements of the blood pool and myocardium. This may serve as a new marker for determining disease burden in amyloid cardiomyopathy.

A direct comparison of ECV determined at 1.5- and 3-T in 31 patients demonstrated similar ECV measurements between these 2 field strengths. However, the investigators noted differences in ECV between the septum and lateral wall, which may be related to susceptibility and will likely be more problematic at higher field strengths (74).

Using the pre- and post-contrast  $T_1$ -maps, one can generate parametric images of Vd which reflect the ECV (Fig. 10), thus providing a new type of image contrast which may provide insight into diseases characterized by regional differences in fibrosis (71). ECV mapping may also have important prognostic significance in different cardiac pathologies (75).

The development of robust techniques for non-rigid registration has greatly improved the clinical applicability of  $T_1$  mapping, as  $T_1$  maps can be generated without the need for user interaction (64). Further developments in parallel and compressed sensing techniques will further improve the spatial and temporal resolution of parametric mapping.

**Potential clinical pitfalls and solutions.** It is important to note that the MOLLI  $T_1$  mapping pulse

sequences have some heart rate dependence which may bias measured  $T_1$  relaxation times particularly in patients with fast heart rates. As this bias is  $T_1$  dependent, the effect is worse for pre-contrast  $T_1$  times where the  $T_1$  relaxation times are on the order of 1 to 1.5 s. For the MOLLI pulse sequence this effect can be mitigated to an extent by increasing the number of relaxation heartbeats; however, this directly increases the required breath-hold. Second, the specific parameters of the SSFP readout module can also introduce some  $T_2$  dependence to the measured  $T_1$  values. Thus, some caution is warranted when comparing  $T_1$  measurements acquired by different methodologies.

**Conclusions.** Quantitative techniques for myocardial perfusion and parametric mapping of magnetic relaxation times are extending the unique potential of CMR for characterization of cardiac structure and physiology. There is a growing body of evidence for the clinical utility of quantitative assessment of perfusion and relaxation times, although current techniques still have some important limitations. There are significant differences in the techniques used for both image acquisition and image analysis between MRI vendors and different sites. Standardization of acquisition and analysis will be important for the wider clinical applicability of these techniques. Improved scanner technology and reconstruction and image processing techniques are rapidly evolving which will further improve the available techniques for CMR parametric mapping. Further research will be necessary to demonstrate that these new techniques will offer incremental diagnostic and prognostic utility and robustness as compared to current visual and semiquantitative CMR techniques.

#### Acknowledgment

The authors would like to acknowledge Robin LeGallo for help with the histological sections.

**Reprint requests and correspondence:** Dr. Christopher M. Kramer, Departments of Medicine and Radiology, University of Virginia Health System, 1215 Lee Street, Charlottesville, Virginia 22908. *E-mail:* ckramer@virginia.edu.

#### REFERENCES

1. Lorenz CH, Walker ES, Morgan VL, Klein SS, Graham TP Jr. Normal human right and left ventricular mass, systolic function, and gender differences by cine magnetic resonance imaging. *J Cardiovasc Magn Reson* 1999;1:7-21.
2. Patel AR, Antkowiak PF, Nandalur KR, et al. Assessment of advanced coronary artery disease: advantages of quantitative cardiac magnetic resonance perfusion analysis. *J Am Coll Cardiol* 2010;56:561-9.
3. Jerosch-Herold M, Sheridan DC, Kushner JD, et al. Cardiac magnetic

- resonance imaging of myocardial contrast uptake and blood flow in patients affected with idiopathic or familial dilated cardiomyopathy. *Am J Physiol Heart Circ Physiol* 2008;295:H1234-42.
4. Iles L, Pfluger H, Phrommintikul A, et al. Evaluation of diffuse myocardial fibrosis in heart failure with cardiac magnetic resonance contrast-enhanced T<sub>1</sub> mapping. *J Am Coll Cardiol* 2008;52:1574-80.
  5. Flett AS, Hayward MP, Ashworth MT, et al. Equilibrium contrast cardiovascular magnetic resonance for the measurement of diffuse myocardial fibrosis: preliminary validation in humans. *Circulation* 2010;122:138-44.
  6. Verhaert D, Thavendiranathan P, Giri S, et al. Direct T<sub>2</sub> quantification of myocardial edema in acute ischemic injury. *J Am Coll Cardiol Img* 2011;4:269-78.
  7. Thavendiranathan P, Walls M, Giri S, et al. Improved detection of myocardial involvement in acute inflammatory cardiomyopathies using T<sub>2</sub> mapping. *Circ Cardiovasc Imaging* 2012;5:102-10.
  8. Anderson LJ, Holden S, Davis B, et al. Cardiovascular T2-star (T<sub>2</sub><sup>\*</sup>) magnetic resonance for the early diagnosis of myocardial iron overload. *Eur Heart J* 2001;22:2171-9.
  9. Tanner MA, Galanello R, Dessi C, et al. A randomized, placebo-controlled, double-blind trial of the effect of combined therapy with deferoxamine and deferiprone on myocardial iron in thalassemia major using cardiovascular magnetic resonance. *Circulation* 2007;115:1876-84.
  10. Berman DS, Kang X, Slomka PJ, et al. Underestimation of extent of ischemia by gated SPECT myocardial perfusion imaging in patients with left main coronary artery disease. *J Nucl Cardiol* 2007;14:521-8.
  11. Christian TF, Miller TD, Bailey KR, Gibbons RJ. Noninvasive identification of severe coronary artery disease using exercise tomographic thallium-201 imaging. *Am J Cardiol* 1992;70:14-20.
  12. Patel AR, Epstein FH, Kramer CM. Evaluation of the microcirculation: advances in cardiac magnetic resonance perfusion imaging. *J Nucl Cardiol* 2008;15:698-708.
  13. Murthy VL, Naya M, Foster CR, et al. Association between coronary vascular dysfunction and cardiac mortality in patients with and without diabetes mellitus. *Circulation* 2012;127:1858-68.
  14. Salerno M, Beller GA. Noninvasive assessment of myocardial perfusion. *Circ Cardiovasc Imaging* 2009;2:412-24.
  15. Morton G, Chiribiri A, Ishida M, et al. Quantification of absolute myocardial perfusion in patients with coronary artery disease: comparison between cardiovascular magnetic resonance and positron emission tomography. *J Am Coll Cardiol* 2012;60:1546-55.
  16. Kellman P, Derbyshire JA, Agyeman KO, McVeigh ER, Arai AE. Extended coverage first-pass perfusion imaging using slice-interleaved TSENSE. *Magn Reson Med* 2004;51:200-4.
  17. Manka R, Vitanis V, Boesiger P, Flammer AJ, Plein S, Kozzerke S. Clinical feasibility of accelerated, high spatial resolution myocardial perfusion imaging. *J Am Coll Cardiol Img* 2010;3:710-7.
  18. Manka R, Jahnke C, Kozzerke S, et al. Dynamic 3-dimensional stress cardiac magnetic resonance perfusion imaging: detection of coronary artery disease and volumetry of myocardial hypoenhancement before and after coronary stenting. *J Am Coll Cardiol* 2011;57:437-44.
  19. Otazo R, Kim D, Axel L, Sodickson DK. Combination of compressed sensing and parallel imaging for highly accelerated first-pass cardiac perfusion MRI. *Magn Reson Med* 2010;64:767-76.
  20. Christian TF, Aletras AH, Arai AE. Estimation of absolute myocardial blood flow during first-pass MR perfusion imaging using a dual-bolus injection technique: comparison to single-bolus injection method. *J Magn Reson Imaging* 2008;27:1271-7.
  21. Gatehouse PD, Elkington AG, Ablitt NA, Yang GZ, Pennell DJ, Firmin DN. Accurate assessment of the arterial input function during high-dose myocardial perfusion cardiovascular magnetic resonance. *J Magn Reson Imaging* 2004;20:39-45.
  22. Larsson HB, Fritz-Hansen T, Rostrup E, Sondergaard L, Ring P, Henriksen O. Myocardial perfusion modeling using MRI. *Magn Reson Med* 1996;35:716-26.
  23. Jerosch-Herold M, Wilke N, Stillman AE. Magnetic resonance quantification of the myocardial perfusion reserve with a Fermi function model for constrained deconvolution. *Med Phys* 1998;25:73-84.
  24. Jerosch-Herold M, Wilke N, Wang Y, et al. Direct comparison of an intravascular and an extracellular contrast agent for quantification of myocardial perfusion. *Cardiac MRI Group. Int J Card Imaging* 1999;15:453-64.
  25. Pack NA, DiBella EV. Comparison of myocardial perfusion estimates from dynamic contrast-enhanced magnetic resonance imaging with four quantitative analysis methods. *Magn Reson Med* 2010;64:125-37.
  26. Zun Z, Varadarajan P, Pai RG, Wong EC, Nayak KS. Arterial spin labeled CMR detects clinically relevant increase in myocardial blood flow with vasodilation. *J Am Coll Cardiol Img* 2011;4:1253-61.
  27. Fritz-Hansen T, Hove JD, Kofoed KF, Kelbaek H, Larsson HB. Quantification of MRI measured myocardial perfusion reserve in healthy humans: a comparison with positron emission tomography. *J Magn Reson Imaging* 2008;27:818-24.
  28. Kurita T, Sakuma H, Onishi K, et al. Regional myocardial perfusion reserve determined using myocardial perfusion magnetic resonance imaging showed a direct correlation with coronary flow velocity reserve by Doppler flow wire. *Eur Heart J* 2009;30:444-52.
  29. Costa MA, Shoemaker S, Futamatsu H, et al. Quantitative magnetic resonance perfusion imaging detects anatomic and physiologic coronary artery disease as measured by coronary angiography and fractional flow reserve. *J Am Coll Cardiol* 2007;50:514-22.
  30. Bernhardt P, Walcher T, Rottbauer W, Wöhrle J. Quantification of myocardial perfusion reserve at 1.5 and 3.0 Tesla: a comparison to fractional flow reserve. *Int J Cardiovasc Imaging* 2012;28:2049-56.
  31. Salerno M, Sica C, Kramer CM, Meyer CH. Improved first-pass spiral myocardial perfusion imaging with variable density trajectories. *Magn Reson Med* 2012 Dec 27 [E-pub ahead of print]
  32. Salerno M, Sica CT, Kramer CM, Meyer CH. Optimization of spiral-based pulse sequences for first-pass myocardial perfusion imaging. *Magn Reson Med* 2011;65:1602-10.
  33. Hsu LY, Groves DW, Aletras AH, Kellman P, Arai AE. A quantitative pixel-wise measurement of myocardial blood flow by contrast-enhanced first-pass CMR perfusion imaging: microsphere validation in dogs and feasibility study in humans. *J Am Coll Cardiol Img* 2012;5:154-66.
  34. Nandalur KR, Dwamena BA, Choudhri AF, Nandalur MR, Carlos RC. Diagnostic performance of stress cardiac magnetic resonance imaging in the detection of coronary artery disease: a meta-analysis. *J Am Coll Cardiol* 2007;50:1343-53.
  35. Westwood M, Anderson LJ, Firmin DN, et al. A single breath-hold multiecho T<sub>2</sub><sup>\*</sup> cardiovascular magnetic resonance technique for diagnosis of myocardial iron overload. *J Magn Reson Imaging* 2003;18:33-9.
  36. Zia MI, Ghugre NR, Connelly KA, et al. Characterizing myocardial edema and hemorrhage using quantitative T<sub>2</sub> and T<sub>2</sub><sup>\*</sup> mapping at multiple time intervals post ST-segment elevation myocardial infarction. *Circ Cardiovasc Imaging* 2012;5:566-72.

37. Wacker CM, Hartlep AW, Pflieger S, Schad LR, Ertl G, Bauer WR. Susceptibility-sensitive magnetic resonance imaging detects human myocardium supplied by a stenotic coronary artery without a contrast agent. *J Am Coll Cardiol* 2003;41:834-40.
38. Manka R, Paetsch I, Schnackenburg B, Gebker R, Fleck E, Jahnke C. BOLD cardiovascular magnetic resonance at 3.0 Tesla in myocardial ischemia. *J Cardiovasc Magn Reson* 2010;12:54.
39. Abdel-Aty H, Zagrosek A, Schulz-Menger J, et al. Delayed enhancement and T2-weighted cardiovascular magnetic resonance imaging differentiate acute from chronic myocardial infarction. *Circulation* 2004;109:2411-6.
40. Abdel-Aty H, Boye P, Zagrosek A, et al. Diagnostic performance of cardiovascular magnetic resonance in patients with suspected acute myocarditis: comparison of different approaches. *J Am Coll Cardiol* 2005;45:1815-22.
41. Vignaux O, Dhote R, Duboc D, et al. Detection of myocardial involvement in patients with sarcoidosis applying T2-weighted, contrast-enhanced, and cine magnetic resonance imaging: initial results of a prospective study. *J Comput Assist Tomogr* 2002;26:762-7.
42. Lund G, Morin RL, Olivari MT, Ring WS. Serial myocardial T<sub>2</sub> relaxation time measurements in normal subjects and heart transplant recipients. *J Heart Transplant* 1988;7:274-9.
43. Foltz WD, Al-Kwif O, Sussman MS, Stainsby JA, Wright GA. Optimized spiral imaging for measurement of myocardial T<sub>2</sub> relaxation. *Magn Reson Med* 2003;49:1089-97.
44. Huang TY, Liu YJ, Stemmer A, Poncelet BP. T<sub>2</sub> measurement of the human myocardium using a T2-prepared transient-state TrueFISP sequence. *Magn Reson Med* 2007;57:960-6.
45. Giri S, Chung YC, Merchant A, et al. T<sub>2</sub> quantification for improved detection of myocardial edema. *J Cardiovasc Magn Reson* 2009;11:56.
46. Aletas AH, Tilak GS, Natanzon A, et al. Retrospective determination of the area at risk for reperfused acute myocardial infarction with T2-weighted cardiac magnetic resonance imaging: histopathological and displacement encoding with stimulated echoes (DENSE) functional validations. *Circulation* 2006;113:1865-70.
47. Ugander M, Bagi PS, Oki AJ, et al. Myocardial edema as detected by pre-contrast T<sub>1</sub> and T<sub>2</sub> CMR delineates area at risk associated with acute myocardial infarction. *J Am Coll Cardiol* 2012;59:596-603.
48. Eitel I, Desch S, Fuernau G, et al. Prognostic significance and determinants of myocardial salvage assessed by cardiovascular magnetic resonance in acute reperfused myocardial infarction. *J Am Coll Cardiol* 2010;55:2470-9.
49. He T, Smith GC, Gatehouse PD, Mohiaddin RH, Firmin DN, Pennell DJ. On using T<sub>2</sub> to assess extrinsic magnetic field inhomogeneity effects on T<sub>2</sub>\* measurements in myocardial siderosis in thalassemia. *Magn Reson Med* 2009;61:501-6.
50. Assomull RG, Prasad SK, Lyne J, et al. Cardiovascular magnetic resonance, fibrosis, and prognosis in dilated cardiomyopathy. *J Am Coll Cardiol* 2006;48:1977-85.
51. Kim RJ, Wu E, Rafael A, et al. The use of contrast-enhanced magnetic resonance imaging to identify reversible myocardial dysfunction. *N Engl J Med* 2000;343:1445-53.
52. Brooks J, Kramer CM, Salerno M. Markedly increased volume of distribution of gadolinium in cardiac amyloidosis demonstrated by T<sub>1</sub> mapping. *J Magn Reson Imaging* 2013 Feb 28 [E-pub ahead of print]; <http://dx.doi.org/10.1002/jmri.24078>.
53. Puntmann VO, Voigt T, Chen Z, et al. Native T<sub>1</sub> mapping in differentiation of normal myocardium from diffuse disease in hypertrophic and dilated cardiomyopathy. *J Am Coll Cardiol* 2013;61:475-84.
54. Karamitsos TD, Piechnik SK, Banyersad SM, et al. Noncontrast T<sub>1</sub> mapping for the diagnosis of cardiac amyloidosis. *J Am Coll Cardiol* 2013;61:488-97.
55. Salerno M, Kramer CM. Evaluation of cardiac amyloidosis with T<sub>1</sub> mapping. Presented at: ISMRM; May 9, 2012; Melbourne, Australia.
56. Broberg CS, Chugh SS, Conklin C, Sahn DJ, Jerosch-Herold M. Quantification of diffuse myocardial fibrosis and its association with myocardial dysfunction in congenital heart disease. *Circ Cardiovasc Imaging* 2010;3:727-34.
57. Flacke S, Allen JS, Chia JM, et al. Characterization of viable and nonviable myocardium at MR imaging: comparison of gadolinium-based extracellular and blood pool contrast materials versus manganese-based contrast materials in a rat myocardial infarction model. *Radiology* 2003;226:731-8.
58. Klein C, Nekolla SG, Balbach T, et al. The influence of myocardial blood flow and volume of distribution on late Gd-DTPA kinetics in ischemic heart failure. *J Magn Reson Imaging* 2004;20:588-93.
59. Nacif MS, Turkbey EB, Gai N, et al. Myocardial T<sub>1</sub> mapping with MRI: comparison of look-locker and MOLLI sequences. *J Magn Reson Imaging* 2011;34:1367-73.
60. Messroghli DR, Greiser A, Frohlich M, Dietz R, Schulz-Menger J. Optimization and validation of a fully-integrated pulse sequence for modified look-locker inversion-recovery (MOLLI) T<sub>1</sub> mapping of the heart. *J Magn Reson Imaging* 2007;26:1081-6.
61. Messroghli DR, Radjenovic A, Kozerke S, Higgins DM, Sivanathan MU, Ridgway JP. Modified Look-Locker inversion recovery (MOLLI) for high-resolution T<sub>1</sub> mapping of the heart. *Magn Reson Med* 2004;52:141-6.
62. Schelbert EB, Testa SM, Meier CG, et al. Myocardial extravascular extracellular volume fraction measurement by gadolinium cardiovascular magnetic resonance in humans: slow infusion versus bolus. *J Cardiovasc Magn Reson* 2011;13:16.
63. Piechnik SK, Ferreira VM, Dall'Armellina E, et al. Shortened Modified Look-Locker Inversion recovery (ShMOLLI) for clinical myocardial T<sub>1</sub>-mapping at 1.5 and 3 T within a 9 heartbeat breathhold. *J Cardiovasc Magn Reson* 2010;12:69.
64. Xue H, Shah S, Greiser A, et al. Motion correction for myocardial T<sub>1</sub> mapping using image registration with synthetic image estimation. *Magn Reson Med* 2012;67:1644-55.
65. Flacke SJ, Fischer SE, Lorenz CH. Measurement of the gadopentetate dimeglumine partition coefficient in human myocardium in vivo: normal distribution and elevation in acute and chronic infarction. *Radiology* 2001;218:703-10.
66. Salerno M, Janardhanan R, Jiji RS, et al. Comparison of methods for determining the partition coefficient of gadolinium in the myocardium using T(1) mapping. *J Magn Reson Imaging* 2012 Nov 29 [E-pub ahead of print]; <http://dx.doi.org/10.1002/jmri.23875>.
67. Piechnik SK, Ferreira VM, Lewandowski AJ, et al. Normal variation of magnetic resonance T<sub>1</sub> relaxation times in the human population at 1.5 T using ShMOLLI. *J Cardiovasc Magn Reson* 2013;15:13.
68. Messroghli DR, Niendorf T, Schulz-Menger J, Dietz R, Friedrich MG. T<sub>1</sub> mapping in patients with acute myocardial infarction. *J Cardiovasc Magn Reson* 2003;5:353-9.
69. Sibley CT, Noureldin RA, Gai N, et al. T<sub>1</sub> mapping in cardiomyopathy at cardiac MR: comparison with endomyocardial biopsy. *Radiology* 2012;265:724-32.
70. Maceira AM, Prasad SK, Hawkins PN, Roughton M, Pennell DJ. Cardiovascular magnetic resonance and prognosis in cardiac amyloidosis. *J Cardiovasc Magn Reson* 2008;10:54.
71. Kellman P, Wilson JR, Xue H, et al. Extracellular volume fraction mapping

- in the myocardium, part 2: initial clinical experience. *J Cardiovasc Magn Reson* 2012;14:64.
72. Green JJ, Berger JS, Kramer CM, Salerno M. Prognostic value of late gadolinium enhancement in clinical outcomes for hypertrophic cardiomyopathy. *J Am Coll Cardiol Img* 2012; 5:370-7.
73. Mongeon FP, Jerosch-Herold M, Coelho-Filho OR, Blankstein R, Falk RH, Kwong RY. Quantification of extracellular matrix expansion by CMR in infiltrative heart disease. *J Am Coll Cardiol Img* 2012;5:897-907.
74. Kawel N, Nacif M, Zavodni A, et al. T<sub>1</sub> mapping of the myocardium: intra-individual assessment of post-contrast T<sub>1</sub> time evolution and extracellular volume fraction at 3T for Gd-DTPA and Gd-BOPTA. *J Cardiovasc Magn Reson* 2012;14:26.
75. Wong TC, Piehler K, Meier CG, et al. Association between extracellular matrix expansion quantified by cardiovascular magnetic resonance and short-term mortality. *Circulation* 2012;126:1206-16.

---

**Key Words:** CMR ■ magnetic resonance ■ MRI ■ quantitative.